Research Square

Preprints are preliminary reports that have not undergone peer review.
They should not be considered conclusive, used to inform clinical practice,
or referenced by the media as validated information.

Vegetation recovery predicts soil carbon storage despite 350 years of metal-smelting legacies

Linee Goswami
linee5.evs@gmail.com
Örebro University
Alf Ekblad
Örebro University
Ingrid Rijk
Örebro University
Dan Kleja
Swedish University of Agricultural Sciences, Alnarp
Michaela Zeiner
Örebro University
Viktor Sjoberg
Örebro University

Article

Keywords: Nemoboreal forest recovery, soil carbon storage, metal-contamination legacy, bryophyte cover, nitrogen cycling, stable isotopes, multivariate analyses, predictive modelling

Posted Date: October 21st, 2026

DOI: https://doi.org/10.21203/rs.3.rs-11276160/v1

License: This work is licensed under a Creative Commons Attribution 4.0 International License. Read Full License

Additional Declarations: No competing interests reported.

Abstract

Metal-smelting legacies alter vegetation, nutrient cycling, and soil carbon (C) storage, but controls on long-term recovery remain unclear. We measured soil C stocks, understory cover, soil and plant $\delta^{13}C$ and $\delta^{15}N$, metal contents, and Cu, Zn, and Pb isotope ratios along a smelter-impact gradient in nemoboreal forests around the Gusum brassworks, Sweden. Depth-resolved sampling and partial least squares regression assessed biological and geochemical predictors of soil C storage. Stocks were lowest near the active smelter and at intermediate sites but highest at reference and historically contaminated sites, showing that recovery did not track distance or metal loads alone. Moss cover and the soil $\delta^{15}N$ depth gradient were the strongest predictors, whereas metal contents and isotope signatures mainly traced contamination history. Thus, soil C storage is more closely associated with recovery of bryophyte-dominated forest floors and depth-organized N cycling than with persistent metal legacies alone.

Introduction

Industrial activities have left long-lasting legacies in terrestrial ecosystems worldwide, altering vegetation structure, nutrient cycling, and soil organic carbon (C) storage (Hutchinson & Whitby, 1977; Helmisaari, 2001; Rijk & Ekblad, 2020). In boreal and nemoboreal forests—among the largest terrestrial C sinks—such disturbances raise critical questions about ecosystem resilience and recovery under global change (Turetsky et al., 2012). Although industrial emissions have declined across much of northern Europe during recent decades, soils and vegetation continue to bear strong imprints of historical exposure (Tyler, 1984; Folkeson & Andersson Bringmark, 1988; Rijk & Ekblad, 2020; Rijk et al., 2026). Consequently, the mechanisms regulating long-term recovery of soil C stocks remain poorly resolved, particularly the relative importance of persistent geochemical contamination versus biological re-establishment.

Soil organic matter formation and persistence reflect coupled plant inputs, microbial transformations, mineral interactions, and environmental constraints (Angst et al., 2025; Rocci et al., 2024). In boreal forests, forest-floor vegetation regulates these processes by modifying microclimate, substrate quality, and nutrient availability (Kleja et al., 2008). Bryophyte carpets are particularly important because they retain moisture, buffer temperature fluctuations, and supply slowly decomposing litter that promotes organic matter accumulation (Kögel-Knabner & Amelung, 2013; Rocci et al., 2024). Sphagnum mosses support major long-term C stores in peat-forming systems (Tamm, 1953; Turetsky et al., 2012), while feather mosses such as *Hylocomium splendens* and *Pleurozium schreberi* influence insulation, litter inputs, and microbial activity in upland boreal forests (Kleja et al., 2008; Eldridge et al., 2023). Moss production can also contribute substantially to soil C sequestration in boreal peatlands (Kasimir et al., 2021), underscoring the need to represent bryophytes explicitly when assessing ecosystem C storage.

Disturbances that suppress bryophyte cover can therefore propagate major effects on soil biogeochemical functioning. Atmospheric deposition from metal smelters provides a particularly strong example. Emissions of copper (Cu), zinc (Zn), and lead (Pb) have historically elevated trace metal contents in forest soils, suppressing bryophytes and restructuring forest floor vegetation (Folkeson, 1981; Hutchinson & Whitby, 1977; Folkeson & Andersson-Bringmark, 1988). In boreal forests, such disturbances often shift ground-layer composition toward graminoids, alter litter quality, and disrupt nutrient cycling, with cascading effects on soil C storage (Kleja et al., 2008; Klaminder, 2004). Importantly, soil C stocks do not always track gradients in metal contents or distance from emission sources alone (Helmisaari, 2001), suggesting that indirect biological controls may dominate long-term ecosystem trajectories.

Identifying robust, process-based indicators of ecosystem recovery remains a key challenge in global change research. Stable isotopes provide powerful integrative tools in this regard. Natural abundance $\delta^{13}C$ reflects plant inputs and decomposition processes, whereas $\delta^{15}N$ integrates fractionating N transformations such as mineralization, nitrification, and N losses (Högberg, 1997; Craine et al., 2015). Critically, the vertical structure of soil $\delta^{15}N$ captures the cumulative imprint of organic matter processing and N cycle openness over time, providing information that cannot be inferred from surface measurements alone (Hobbie & Ouimette, 2009; Kramer et al., 2017). Meta-analyses further indicate that soil $\delta^{15}N$ is a

stronger indicator of the state of ecosystem N cycling than plant $\delta^{15}N$ in forest systems (Templer et al., 2007; Liao et al., 2021). By contrast, soil metal contents and stable metal isotope ratios primarily trace contamination sources, transport, and mixing (Bindler et al., 1999; Brännvall et al., 2001; Klaminder et al., 2004; Wiederhold, 2015), and their explanatory power for ecosystem C storage relative to biological indicators remains uncertain.

The forests surrounding the Gusum Brassworks in southeastern Sweden provide a unique opportunity to disentangle these controls. More than three centuries of brass production have generated pronounced gradients of Zn, Cu, and Pb in the surrounding coniferous forest soils, accompanied by well-documented changes in forest-floor vegetation and soil chemistry (Tyler, 1984; Folkeson & Andersson-Bringmark, 1988; Langemar, 1994). Early studies reported severe suppression of bryophytes and lichens near emission sources, with gradual recovery following reduced emissions (Folkeson, 1981; Folkeson & Andersson-Bringmark, 1988). However, despite extensive characterization of contamination patterns, the mechanisms governing contemporary variation in soil C storage across this landscape remain unresolved.

Here, we investigate soil C storage, nitrogen (N) cycling, and vegetation structure along a smelter-impact gradient surrounding the Gusum Brassworks by integrating vegetation surveys, depth-resolved soil and plant $\delta^{13}C$ and $\delta^{15}N$ measurements, soil metal contents, and stable metal isotope ratios. Using partial least squares regression (PLS) (Wold et al., 2001), we evaluate the relative importance of biological indicators of recovery—particularly moss and understory vegetation cover and depth-resolved isotopic structure—versus geochemical contamination proxies for explaining variation in soil C stocks. In contrast to multiple regression analyses, PLS can handle correlated X-variables and extract relevant information out of such data (Ref).

We hypothesized that (i) soil C storage would be more strongly associated with indicators of vegetation recovery than with trace-metal contents or metal isotope signatures alone, and (ii) the vertical gradient of soil $\delta^{15}N$ would provide a robust, integrative indicator of soil biogeochemical recovery.

Results

Soil metal contents and metal isotope signatures

Metal contents varied strongly across sites and depths (Table 2 and Supplementary Table 3a). At 5–10 cm, Zn had an ANOVA F value of 47.92, with the highest mean at the new smelter site (9200.38 mg kg^{-1}) and the lowest at the reference site (622.27 mg kg^{-1}), a difference of 8578.11 mg kg^{-1}. Cu at 5–10 cm had an ANOVA F value of 32.14, with the maximum concentration at the old smelter site (10019.16 mg kg^{-1}) and the minimum at the reference site (165.89 mg kg^{-1}), giving a site-to-site difference of 9853.27 mg kg^{-1}. Pb did not show statistically significant differences at any depth band, although the largest site contrast also occurred at 5–10 cm, where Pb ranged from 146.07 mg kg^{-1} at the reference site to 1200.93 mg kg^{-1} at the old smelter site.

Table 2
Soil total metal content (Zn, Cu, and Pb) in mg kg-1 for each site group, with their statistical analyses, reported for L2 (i.e., 5–10 cm of soil). Similarly, metal isotopes, as representative contamination proxies, are reported for L2 with their statistical analyses.

Depth band	Groups						
	New Site	Old Site	Intermediate 1	Intermediate 2	Reference	ANOVA F	Significant
	1 (N = 5)	2 (N = 6)	3 (N = 5)	4 (N = 6)	5 (N = 6)		
Zn 5–10 (mg kg^{-1})							
Mean (SD)	9200 (3107)	8214 (1209)	1347 (379)	1019 (408)	622 (314)	47.92	Yes
Cu 5–10 (mg kg^{-1})							
Mean (SD)	9409 (4310)	10019 (2496)	589 (140)	314 (216)	165 (84)	32.14	Yes
Pb 5–10 (mg kg^{-1})							
Mean (SD)	461 (257)	1200 (899)	306 (110)	242 (140)	146 (108)	5.45	No
Cu 65_63_L2							
Mean (SD)	0.481 (0.008)	0.486 (0.005)	0.482 (0.008)	0.479 (0.005)	0.477 (0.008)	1.48	No
Zn67_66_L2							
Mean (SD)	0.151 (0.0008)	0.150 (0.0006)	0.154 (0.003)	0.153(0.003)	0.157 (0.006)	3.35	No
Pb 206_207_L2							
Mean (SD)	1.224 (0.021)	1.175 (0.006)	1.243 (0.092)	1.230 (0.070)	1.148 (0.022)	3.429	No

Depth profiles showed distinct percentage changes among the new smelter, old smelter, and reference sites (Supplementary Table 4). For the statistically significant Zn result at 5–10 cm, the depth pattern showed a strong decline through the soil profile at the new smelter site, decreasing by 51% from 0–5 to 5–10 cm and by a further 33% from 5–10 to 10–20 cm, equivalent to a 67% decline from the surface to 10–20 cm. At the old smelter site, Zn declined more gradually, by 10% and then 23%, giving an overall 31% decrease. At the reference site, Zn decreased by 43% from 0–5 to 5–10 cm and by 44% from 5–10 to 10–20 cm, resulting in the largest overall decline among the reference profiles (-68%).

For the statistically significant Cu result at 5–10 cm, the new smelter site showed a small decline from 0–5 to 5–10 cm (-9%) followed by a sharper decrease from 5–10 to 10–20 cm (-62%), producing an overall 65% reduction across the soil profile. In contrast, the old smelter site showed a pronounced subsurface enrichment: Cu increased by 100% from 0–5 to 5–10 cm, then decreased by 17% at 10–20 cm, resulting in a net 67% increase from the surface to the deepest layer. At the reference site, Cu decreased consistently with depth (-18% and – 39%), with an overall 50% reduction. Pb was not statistically significant, but its depth pattern contrasted with Cu and Zn: Pb decreased strongly at the new smelter site (-33%, then – 65%;

overall − 77%), increased at the old smelter site from 0–5 to 5–10 cm (+ 98%) before declining at 10–20 cm (-38%; overall + 23%), and showed only a small net increase at the reference site (+ 3%) despite a 37% decline between 5–10 and 10–20 cm.

Isotopic signatures

Metal isotope ratios showed no statistically significant site-level differences across the soil profile (Table 2 and Supplementary Table 3b). For $^{65}Cu/^{63}Cu$, ANOVA F values were low at all layers (L1 = 0.27, L2 = 1.48, L3 = 0.89). Mean ratios varied narrowly among sites, from 0.479 to 0.483 at L1, 0.477 to 0.486 at L2, and 0.480 to 0.485 at L3. The largest site-to-site spread was therefore only 0.009 at L2, indicating that Cu isotope signatures were much less differentiated than Cu contents.

For $\delta^{67}/^{66}Zn$, site differences were also non-significant across all layers (Table 2 and Supplementary 3b; ANOVA F = 3.01 at L1, 3.35 at L2, and 6.16 at L3). The ratios ranged from 0.150 to 0.155 at L1, 0.150 to 0.157 at L2, and 0.150 to 0.156 at L3. Although the highest F value occurred at L3, the absolute differences among sites remained small, with maximum spreads of 0.005, 0.007, and 0.006 across L1, L2, and L3, respectively.

For $^{206}Pb/^{207}Pb$, there were no statistically significant differences between depths or between the groups at any depth layer (Table 2 and Supplementary Table 3b).

Interestingly, neither absolute metal contents nor metal isotope ratios showed a clear correspondence with spatial variation in soil C stocks when considered independently (Supplementary Fig. 2).

Soil carbon and nitrogen stocks

Consistent and statistically significant among-site variation in carbon stock was found across all depth bands and for the total 0–20 cm profile (Table 3). In the 0–5 cm layer, carbon stock was highest at the Reference group (4245.49 g m^{-2}) and lowest at Intermediate 1 (1010.70 g m^{-2}, representing a 320.1% increase at the Reference group ($F = 11.214$, $p < 0.001$). The same pattern was evident at 5–10 cm, where the Reference group (2622.97 g m^{-2}) exceeded Intermediate 1 (836.62 g m^{-2} by 213.5% ($F = 14.896$, $p < 0.001$). In contrast, the deepest band showed a shift in the maximum value: the Old Site group had the highest C stock at 10–20 cm (1755.70 g m^{-2}) exceeding the New Site group (620.70 g m^{-2}) by 182.8% ($F = 4.037$, $p = 0.0127$). Across the full 0–20 cm profile, total C stock was greatest at the Old Site (8442.73 g m^{-2}), and lowest at Intermediate 1 (2483.11 g m^{-2}), a 239.9% difference ($F = 17.167$, $p < 0.001$).

Table 3

Soil carbon and nitrogen stocks and stable isotope composition across restoration distance gradient sites. Values are reported as mean (SD) for each site category, including New Site, Old Site, Intermediate 1, Intermediate 2, and Reference sites. The table summarizes depth-specific and total carbon stocks, depth-specific and total nitrogen stocks, and stable isotope signatures of carbon and nitrogen across soil depth bands. ANOVA F statistics and corresponding P values are provided to evaluate among-site differences, with * denoting statistically significant differences and ns denoting non-significant effects.

Parameter		New Site	Old Site	Intermediate 1	Intermediate 2	Reference	ANOVA F	p-value	Sig.
		1	2	3	4	5			
		(N = 5) (SE)	(N = 6) (SE)	(N = 5) (SE)	(N = 6) (SE)	(N = 6) (SE)			
C stock (g/m²)									
Mean (SD)	Depth band								
	0–5 cm	1486 (633.44)	4230 (2008.96)	1010 (565.77)	1395 (414.73)	4245 (1156.09)	11.214	3.398E-05	*
	5–10 cm	1096 (328.30)	2456 (926.59)	836 (252.41)	998 (414.80)	2623 (376.53)	14.896	3.837E-06	*
	10–20 cm	621 (606.92)	1756 (737.76)	636 (458.42)	643 (408.37)	1008 (630.87)	4.0367	0.01267	*
Total C stock (g/m²) Mean (SD)		3204 (950.61)	8443 (2821.59)	2483 (1119.27)	3037 (526.39)	7877 (1681.58)	17.167	1.195E-06	*
N stock (g/m²)									
Mean (SD)	Depth band								
	0–5 cm	56.93 (21.88)	145.00 (65.76)	39.36 (26.39)	49.89 (12.23)	139.84 (34.17)	10.651	4.933E-05	*
	5–10 cm	56.32 (11.39)	89.77 (34.17)	36.79 (16.89)	36.38 (15.35)	82.55 (17.96)	8.0618	0.00032	*
	10–20 cm	24.58 (19.28)	71.17 (29.41)	29.83 (28.89)	22.57 (14.41)	30.20 (17.18)	4.707	0.00636	*
Total N stock (g/m²) Mean (SD)		137.83 (31.36)	305.94 (92.94)	105.99 (67.54)	108.83 (19.28)	252.59 (55.84)	13.347	9.14E-06	*
δ13C (‰)									
Mean (SD)	Depth band								
	0–5 cm	-28.30 (0.89)	-27.97 (0.36)	-28.14 (0.55)	-27.85 (0.38)	-27.67 (0.19)	1.286	0.304	ns
	5–10 cm	-27.53 (0.35)	-27.58 (0.26)	-27.31 (0.48)	-27.44 (0.47)	-26.89 (0.29)	3.118	0.0345	*
	10–20 cm	-27.18 (0.36)	-26.99 (0.23)	-27.01 (0.51)	-26.89 (0.29)	-26.53 (0.30)	2.743	0.0531	ns
δ15N (‰)									

Parameter		New Site	Old Site	Intermediate 1	Intermediate 2	Reference	ANOVA F	p-value	Sig.
		1	2	3	4	5			
		(N = 5) (SE)	(N = 6) (SE)	(N = 5) (SE)	(N = 6) (SE)	(N = 6) (SE)			
Mean (SD)	Depth band								
	0–5 cm	-2.40 (0.93)	-3.43 (0.22)	-1.55 (2.16)	-3.32 (1.32)	-3.63 (0.64)	2.835	0.0477	*
	5–10 cm	0.38 (1.14)	-2.08 (0.71)	-0.89 (1.76)	-2.97 (1.34)	-1.27 (0.98)	5.883	0.0020	*
	10–20 cm	1.95 (0.84)	1.23 (0.92)	0.21 (2.33)	-1.45 (0.75)	0.81 (1.03)	5.817	0.0021	*

The depth distribution of C stock further indicated that significant differences were driven by both surface accumulation and deeper retention. Carbon stock declined from 0–5 to 10–20 cm by 58.2% at the New Site, 58.5% at the Old Site, 37.1% at Intermediate 1, 53.9% at Intermediate 2, and 76.2% at the Reference Site. Thus, although the Reference site had the largest C stock in the two upper depth bands, its steep vertical decline meant that the Old Site retained the highest total C stock across the full profile.

Nitrogen stock also differed significantly among sites at every depth and for the total profile. In the 0–5 cm layer, the Old Site group had the highest N stock (145.00 g m^{-2}), which was 268.4% higher than Intermediate 1 (39.36 g m^{-2}; $F = 10.651$, $p < 0.001$). At 5–10 cm, the Old Site group again had the highest value (89.77 g m-2), exceeding Intermediate 2 (36.38 g m^{-2}) by 146.8% ($F = 8.062$, $p < 0.001$). At 10–20 cm, the Old Site group (71.17 g m^{-2}) exceeded Intermediate 2 (22.57 g m^{-2}) by 215.3% ($F = 4.707$, $p = 0.00636$). Total N stock followed the same pattern, with the Old Site (305.94 g m^{-2}) exceeding Intermediate 1 (105.99 g m^{-2}) by 188.7% ($F = 13.347$, $p < 0.001$).

Across depth, N stocks decreased in all groups, but the magnitude of decline differed strongly among sites. From 0–5 to 10–20 cm, N stock declined by 56.8% at the New Site, 50.9% at the Old Site, 24.2% at Intermediate 1, 54.8% at Intermediate 2, and 78.4% at the Reference Site. The Old Site therefore combined high surface N stock with comparatively stronger retention at depth, producing the highest total N stock.

Soil $\delta^{13}C$ and $\delta^{15}N$ signatures along the gradient

Bulk soil $\delta^{13}C$ values varied little among sites and site groups (Table 3). Across depth intervals, mean $\delta^{13}C$ values were close to − 28‰ and became less negative with depth, from − 28.0 ± 0.52‰ in the 0–5 cm layer to − 26.91 ± 0.39‰ at 10–20 cm.

For stable isotope composition, statistically significant $\delta^{13}C$ differences were detected only at 5–10 cm ($F = 3.118$, $p = 0.0345$). At this depth, the Reference site was least depleted (− 26.89‰), whereas the Old Site was most depleted (− 27.58‰), giving a 0.69‰ separation among groups. Because isotope values are expressed in per mil units, these differences are reported as absolute shifts rather than percentage changes. The non-significant $\delta^{13}C$ differences at 0–5 cm and 10–20 cm indicate that the significant isotopic separation was restricted to the intermediate depth band.

In contrast, δ15N differed significantly among sites at all depths. At 0–5 cm, values ranged from − 3.63‰ at the reference group to -1.55‰ at Intermediate 1, a 2.08‰ difference ($F = 2.835$, $p = 0.0477$). At 5–10 cm, the New Site group was most enriched (0.38‰), while Intermediate 2 was most depleted (-2.97‰), producing a 3.35‰ spread ($F = 5.883$, $p = 0.0020$). At 10–20 cm, the New Site group remained most enriched (1.95‰), whereas Intermediate 2 remained most depleted (-1.45‰), giving a 3.40‰ separation ($F = 5.817$, $p = 0.0021$). These significant depth-specific contrasts indicate persistent among-site differences in N isotopic composition across the soil (Table 3).

Vegetation structure and recovery patterns

Vegetation structure differed markedly among site groups along the contamination gradient (Fig. 2), and comparison with historical surveys indicates substantial but spatially uneven recovery over four decades. In 1974-75, *Hylocomium splendens* was absent within approximately 1.5 km of the foundry, epiphytic vegetation was strongly reduced within 2–3 km, and moss cover at more distant sites was generally only 20–50% (Folkeson, 1981, 1984). Surveys conducted in the 1980s likewise recorded a severely impoverished inner zone, where ground-layer cover fell from the typical 25–90% to less than 1% near the mills across distance zones extending from 0 to 7 km (Folkeson & Andersson-Bringmark, 1988) (Supplementary Fig. 3). In the present study, the New Site, adjacent to the newer active smelter and within the formerly most affected 0–1.5 km zone, still had the lowest mean moss cover (12 ± 14%) and low shrub cover, indicating incomplete recovery. By contrast, the Old Site, approximately 1.6 km from the new smelter, supported moss cover at the upper end of the observed 83–100% range and a well-developed shrub understory despite high residual soil Cu and Pb (Fig. 2). Intermediate 1 and Intermediate 2 also supported high moss cover (83–100%). However, greater within-group variability and relatively sparse shrub cover indicated patchy re-establishment. At the Reference Site, 7–8 km from the new smelter, moss cover approached 90–100% and shrubs were most consistently developed. The present pattern is therefore not a simple monotonic response to distance: vegetation remains most suppressed beside the newer smelter but has recovered to near-reference structure at the historically contaminated Old Site, with substantial yet heterogeneous recovery at intermediate sites.

Table 1

Sampling: Description of sampling groups and selected sites. Coordinates, including site coordinates, distance, bearing, and cardinal direction, are reported relative to the new smelter. The five Site-group labels used consistently throughout the manuscript are New Site, Old Site, Intermediate 1, Intermediate 2, angular position, and Reference. Distances are expressed in kilometres relative to the text, figures, and bearings in degrees. Replicate sampling points within each site group are described in the Methods. (More information in Fig. 1).

Group	Description	Site	Coordinates	Distance to new smelter (km)	Angle (°)	Direction from new smelter
1	New smelter	7	58.27668, 16.47731	0.505	0	North
		8	58.27664, 16.47758	0.494	0	North
		9	58.27666, 16.47837	0.488	0	North
		10	58.27657, 16.47819	0.481	0	North
		11	58.27623, 16.47825	0.443	0	North
2	Old smelter	1	58.26862, 16.49766	1.15	111	East
		2	58.26849, 16.49774	1.16	113	East
		3	58.26852, 16.49789	1.16	113	East
		4	58.26850, 16.49821	1.18	113	East
		5	58.26844, 16.49835	1.19	114	East
		6	58.26811, 16.49873	1.23	115	East
3	Intermediate1	12	58.273647, 16.455374	1.33	276	West
		13	58.273717, 16.454738	1.38	276	West
		14	58.273381, 16.454428	1.40	276	West
		18	58.281508, 16.501151	1.67	55	North East
		19	58.281949, 16.499667	1.63	55	North East
4	Intermediate2	15	58.279361, 16.442357	2.22	290	NorthWest
		16	58.279361, 16.442358	2.22	290	NorthWest
		17	58.279361, 16.442359	2.22	290	NorthWest
		20	58.254570, 16.455163	2.40	217	Southwest

Group	Description	Site	Coordinates	Distance to new smelter (km)	Angle (°)	Direction from new smelter
		21	58.260121, 16.522342	2.90	120	East_SouthEast
		22	58.260440, 16.522068	2.86	120	SouthEast
5	Reference	23	58.32862, 16.39700	7.82	325	NorthWest
		24	58.32848, 16.39834	7.76	325	NorthWest
		25	58.31738, 16.37692	7.80	310	NorthWest
		26	58.31666, 16.37454	7.86	310	NorthWest
		27	58.31510, 16.37114	7.91	310	NorthWest
		28	58.31412, 16.36888	7.87	309	NorthWest

Moss layer contribution:

Moss variables differed strongly among sites, with significant site effects for moss coverage, $\delta^{13}C$, $\delta^{15}N$, Zn, Cu, and Pb (Supplementary Table 5). Moss coverage showed the clearest site gradient ($F = 122.105$, $p < 0.0001$), being lowest at the New Site groups (12 ± 14%) and much higher at the Old Site groups, Intermediate 1, Intermediate 2, and Reference groups (83–100%). Moss $\delta^{13}C$ also varied significantly among sites ($F = 11.032$, $p < 0.0001$), with the New Site group having the least negative values (-29.8 ± 1.3‰), while the Old Site group was the most depleted (-33.2 ± 0.8‰). Moss $\delta^{15}N$ followed a similar significant site pattern ($F = 10.97$, $p < 0.0001$), with the New Site group enriched relative to the other sites (-3.48 ± 0.85‰) and the Reference group showing the most depleted values (-6.92 ± 0.72‰).

For moss metal concentrations, all three metals showed significant differences among sites (Fig. 2 and Supplementary Table 5). Zn varied significantly ($F = 4.73$, $p = 0.0066$), with the highest mean concentration at the New Site group (1244 ± 1286 μg g^{-1} dw), declining sharply through the Old Site group (212 ± 33 μg g^{-1} dw), Intermediate 1 (125 ± 33 μg g^{-1} dw), Intermediate 2 (93.6 ± 35.8 μg g^{-1} dw), and Reference group (88.8 ± 22.7 μg g^{-1} dw). Cu showed an even stronger site effect ($F = 13.59$, $p < 0.0001$), with the New Site (253 ± 157 μg g^{-1} dw) greatly elevated compared with all other sites (12.9–33.2 μg g^{-1} dw). Pb was also significantly different among sites ($F = 7.82$, $p = 0.0004$), again peaking at the New Site groups (36.7 ± 30.3 μg g^{-1} dw) and remaining low at the Old, intermediate, and reference site groups (2.14–3.45 μg g^{-1} dw). Overall, moss results indicate a strong site-associated decline in metal concentrations from the New Site toward the reference conditions.

Spruce needle contribution:

Spruce needles also showed significant among-site variation, but the pattern differed from moss (Supplementary Table 6). Needle $\delta^{13}C$ varied significantly among sites ($F = 3.57$, $p = 0.0215$), with more negative values at the new and old sites (-30.76 ± 1.02‰ and − 30.63 ± 0.79‰, respectively) and less negative values at the Intermediate 2 and Reference sites (-29.20 ± 0.70‰ and − 29.53 ± 0.76‰, respectively). Needle $\delta^{15}N$ showed a stronger site effect ($F = 5.64$, $p = 0.0030$), declining from relatively enriched values at the new and old sites (-2.69 ± 1.722‰ and − 2.89 ± 2.37‰) to more depleted values at Intermediate 2 and Reference sites (-5.78 ± 0.75‰ and − 6.29 ± 1.23‰). Needle Zn also differed significantly among sites ($F = 3.51$, $p = 0.023$), with the highest mean at the Old Site (122 ± 74 μg g^{-1} dw), followed by Intermediate 1 and the New

Site, and the lowest mean at the Reference site (41.5 ± 16.9 µg g^{-1} dw). In contrast, needle Cu and Pb did not differ significantly among sites (Cu: p = 0.85; Pb: p = 0.182), indicating that the strongest site-related changes in spruce needles were reflected in isotopic composition and Zn rather than Cu or Pb.

PLSR model performance for multivariate predictors of soil carbon storage

Partial least squares regression models for ln-transformed whole-profile soil C stock (0–20 cm) is presented in Table 4. None of the five predictors produced a significant model when used alone. Among models excluding moss and shrub cover, the model containing the two metal-isotope variables was significant (Q^2 = 0.41), indicating that contamination history explained some variation in soil C storage. The model combining moss cover, shrub cover, and soil $\delta^{15}N$ slope had substantially greater predictive ability (Q^2 = 0.64), and adding the two metal-isotope variables produced the highest predictive ability (Q^2 = 0.68). The retained predictors were soil $\delta^{15}N$ slope, $\delta^{67/66}Zn$, $^{206}Pb/^{207}Pb$, moss cover (arcsine transformed), and shrub cover (arcsine transformed); all regression coefficients were positive. Soil $\delta^{15}N$ slope had the highest VIP score, while the remaining predictors had lower and similar values. The final model had R^2X = 0.346, R^2Y = 0.717, and Q^2 = 0.677. Because VIP values depend on covariance among predictors, comparison among model structures provides stronger evidence than any single coefficient; biological indicators and metal-isotope tracers contributed complementary information.

Table 4

Explained predicted variance Q^2(cum) for the different PLS models for C stock of the whole soil layer (0–20 cm depth) using different sets of X predictors. The final selected model is marked in bold. * ln-transformed before centering and scaling.

X	nX	Shrub cover (Tr)	Moss Cover (Tr)	$\delta^{15}N$ slope (‰)	$\delta^{13}C$ slope (‰)	$\delta^{67/66}Zn$ 5–10 cm	$\delta^{206/207}$ Pb 5–10 cm	R2X(cum)	R2Y(cum)	Q2(cum)
ln C stock 0–20 cm (g m^{-2})	**5**	**X**	**X**	**x**		**X**	**x**	**0.358**	**0.725**	**0.685**
	3	X	X	x				0.449	0.656	0.641
	4	X	X	x			x	0.407	0.668	0.621
	2		X	x				0.521	0.641	0.617
	4	X	X			X	x	0.413	0.555	0.488
	2	X		x				0.663	0.443	0.419
	2					x	x	0.483	0.437	0.406
	2	X	X					0.569	0.425	0.361
	1		X					ns	ns	ns
	1	X						ns	ns	ns
	1			x				ns	ns	ns
	1						x	ns	ns	ns
	1					x		ns	ns	ns

Coefficient and VIP analyses supported the model comparison is presented in Table 5. The retained predictors were soil $\delta^{15}N$ slope, $\delta^{67/66}Zn$, $^{206}Pb/^{207}Pb$, moss cover, and shrub cover, and all regression coefficients were positive. Soil $\delta^{15}N$ slope had the highest VIP score, whereas the other retained predictors had lower, similar scores. The final model had R^2X = 0.346, R^2Y = 0.717, and Q^2 = 0.677 (Fig. 3). Because VIP values depend on covariance among predictors, these results do not assign a

dominant mechanism to one variable; instead, they show that vegetation metrics, depth-resolved N-isotope structure, and metal-isotope tracers contributed complementary predictive information (Supplementary Figs. 4 and 5).

Table 5

Summary of the final PLSR model outputs, regression intercepts and coefficients (scaled and centered), and Variable Importance for the Projection (VIP) to summarize the importance of each X variable. R^2X - Fraction of X variation modeled in the component. R^2Y - Fraction of Y variation modeled in the component. Q^2 - Overall cross-validated R^2 for the component. Since the final models have only a single PLS component, the R^2X, R^2Y, and Q^2 are equal to the cumulative (cum) R^2X, R^2Y, and Q^2. VIP-values larger than 1 indicate more "important" X-variables. *ln transformed before centering and scaling.

Y	nX	R^2X (cum)	R^2Y (cum)	Q^2 (cum)	Regr. intercept Y_{avg}	X variable	Unit	Regr. coefficient (± SE)	VIP (± SE)
ln C stock 0–20 cm (g m^{-2})	5	0.358	0.725	0.685	2.301	$\delta^{15}N$ slope	δ^{15} N cm^{-1} soil depth	0.348 (± 0.078)	1.220 (± 0.192)
						$\delta^{67/66}$ Zn (5–10 cm)	‰ depth	0.263 (± 0.026)	0.921(± 0.150)
						Shrub cover (Tr)	%	0.250 (± 0.135)	0.877 (± 0.466)
						Moss cover (Tr)	%	0.299 (± 0.061)	1.049 (± 0.227)
						$\delta^{206/207}$ Pb (5–10 cm)	‰	− 0.253 (± 0.079)	0.888 (± 0.269)

Y	nX	R^2X (cum)	R^2Y (cum)	Q^2 (cum)	Regr. intercept Y_{avg}	X variable	Unit	Regr. coefficient (± SE)	VIP (± SE)

At each site, replicate plots were established to capture local heterogeneity in vegetation and soil properties (Supplementary Fig. 1). This gradient-based design provided the framework for field surveys and sample collection and allowed us to evaluate how soil carbon (C) storage varied in relation to biological recovery and geochemical contamination under long-term industrial disturbance (Helmisaari, 2001; Rijk & Ekblad, 2020).

The final design comprised forest sites assigned to five groups, grouped based on the distance to the new smelter (within brackets). The groups were *New Site* (< 0.5 km), *Old Site* (1-1.2 km), *Intermediate* 1 (1–2 km), *Intermediate* 2 (2–3 km), and *Reference* (7–8 km)—with five to six sampling sites established within each group (Table 1, Fig. 1). This structure allowed group-level comparisons along the contamination gradient while retaining within-group replication for vegetation and soil measurements. All sampling points were located at least 200 m from the E22 national highway to minimize potential road-related influences (Table 1).

Field sampling and sample processing

Field survey and soil sampling

Soils, mosses, and spruce needles were sampled during several campaigns between October and November 2022 and in April 2023.

Soil depths were shallow and varied within each site; a metal rod was used to identify areas with soil at least 20 cm deep. Soil samples were collected using a soil corer with an inner diameter of 50 mm. Before coring, the superficial layer of mosses, lichens, and mixed litter was gently removed where present. Soil cores were collected from either three or four directions (based on the topography) around a mature Norway Spruce tree. Each core was divided into 0–5, 5–10, and 10–20 cm intervals, and core sections were pooled in depth intervals, giving a composite sample from 3–4 cores for each depth. Back in the lab, the pooled soil samples were sieved through a 2 mm mesh, and coarse roots and stones were removed by hand.

Collection of moss and spruce needles and assessment of vegetation composition

Targeted moss and spruce-needle sampling and vegetation composition were conducted on 20–21 April 2023, following approaches previously applied in the Gusum area. At each sampling point, the same tree that was used for soil sampling was also visited for needle collection (ca 100 g per tree) and moss sampling. Around the tree, a 5 × 5 m quadrat was established. Within each quadrat, the cover of the dominant moss species *Hylocomium splendens* (Hedw.) Schimp. and *Pleurozium schreberi* (Brid.) Mitt was recorded, while other moss species were grouped as “other.” The cover of *Vaccinium myrtillus* L., *Vaccinium vitis-idaea* L., and *Deschampsia flexuosa* (L.) Trin. was also recorded when present.

Moss specimens were collected within 2 m of the centrally located Norway spruce tree in each quadrat. Specimens for laboratory identification were collected separately following standard taxonomic procedures. For chemical analysis, *Hylocomium splendens* (Hedw.) Schimp. was sampled using a fixed-area box (14.4 × 18.4 cm) and stored in airtight polypropylene bags. Stand-structure variables recorded for each quadrat included counts of *Picea abies* (L.) H.Karst. and *Pinus sylvestris* L. trees, basal area, tree height, diameter at breast height, light influx, ground-layer vegetation cover, and visually estimated crown cover.

Stable carbon and nitrogen isotope analyses

Stable carbon ($\delta^{13}C$) and nitrogen ($\delta^{15}N$) isotope compositions were measured for soil and plant materials to characterize organic matter inputs and nitrogen (N) cycling processes and to derive depth-resolved isotope indicators for the statistical analyses.

Carbon (C) and nitrogen (N) concentrations and stable isotope ratios ($\delta^{13}C$ and $\delta^{15}N$) of soil and plant samples were determined using elemental analysis coupled to isotope ratio mass spectrometry (EA-IRMS), following established procedures for ecological and biogeochemical studies (Högberg, 1997; Boström et al., 2007). Freeze-dried soil samples and oven-dried plant materials were finely ground before analysis. Subsamples of approximately 2.5 mg for plant material and 5–10 mg for soil were weighed into tin capsules.

Analyses were conducted using a Vario PYRO cube elemental analyzer (Elementar Analysen system GmbH, Germany) coupled online to an Isoprime precisION isotope ratio mass spectrometer (Elementar UK Ltd.). Carbon and nitrogen isotope ratios are reported in delta notation (‰) relative to Vienna Pee Dee Belemnite (VPDB) for $\delta^{13}C$ and atmospheric N_2 for $\delta^{15}N$, respectively.

Instrument calibration was performed using international reference materials IAEA-CH-6 (sucrose) for carbon and IAEA-N-1 (ammonium sulfate) for nitrogen, consistent with recommended isotope normalization protocols (Craine et al., 2015). Wheat flour was used as a laboratory working standard and analysed repeatedly throughout analytical runs. Analytical precision, expressed as the standard deviation of repeated working-standard measurements, was better than ± 0.25‰ for $\delta^{13}C$ and ± 0.10‰ for $\delta^{15}N$.

Y	nX	R^2X (cum)	R^2Y (cum)	Q^2 (cum)	Regr. intercept Y_{avg}	X variable	Unit	Regr. coefficient (± SE)	VIP (± SE)
Elemental C and N concentrations were obtained simultaneously during isotope analysis and used for soil C stock calculations, in line with standard approaches for boreal forest soils (Kleja et al., 2008).									
Soil C and N stocks for each depth interval were calculated from measured elemental concentrations and oven-dry soil mass per unit area after removal of coarse roots and stones. Whole-profile stocks were obtained by summing the 0–5, 5–10, and 10–20 cm intervals.									
Soil and plant metal content analyses									
Sample preparation and digestion									
Soil samples were freeze-dried, homogenized, and finely ground before digestion. Approximately 0.5 g of soil was digested by microwave-assisted acid digestion using suprapure nitric acid (HNO_3) and hydrochloric acid (HCl), following protocols commonly applied in trace-metal studies of contaminated forest soils (Bindler et al., 1999; Brännvall et al., 2001).									
Moss (*Hylocomium splendens* (Hedw.) Schimp.)) and spruce needle samples were gently washed with dilute nitric acid to remove surface contamination, oven-dried, homogenized, and digested using concentrated nitric acid with hydrogen peroxide, following established procedures for vegetation metal analysis near smelters (Folkeson, 1981; Klaminder et al., 2004).									
ICP-MS analysis									
Metal contents were determined using inductively coupled plasma mass spectrometry (ICP-MS; Agilent 7500 series, Agilent Technologies, Japan). External calibration was performed using multi-element standard solutions spanning the concentration ranges observed in the samples. Rhodium (^{103}Rh) was used as an internal standard to correct for instrumental drift and matrix effects (Supplementary Table 1a).									
Quality control included analysis of procedural blanks, replicate digestions, and certified reference materials, consistent with best practice for environmental metal analysis (Bindler et al., 1999; Klaminder, 2004). Instrument performance was monitored through repeated analyses of calibration standards and internal standards throughout analytical sequences.									
Total contents of Cu, Zn, and Pb were used as indicators of smelter-derived contamination intensity.									
Stable metal isotope analyses									
Stable isotope ratios of Cu, Zn and Pb were analysed on selected soil samples to trace contamination sources and mixing between anthropogenic and background metal pools, following established applications of metal isotopes in contaminated forest environments (Brännvall et al., 2001; Wiederhold, 2015).									
Zinc isotope ratios are reported as $\delta^{67}/^{66}Zn$ relative to the JMC-Lyon Zn standard, while lead isotope ratios are reported as $^{206}/^{207}Pb$. Instrumental mass bias was corrected using standard–sample bracketing, and analytical reproducibility was assessed through repeated measurements of standards and selected samples (Supplementary Table 1b).									
Metal isotope ratios were interpreted as qualitative geochemical tracers of contamination sources and were not used for quantitative mass-balance calculations (Klaminder et al., 2004; Wiederhold, 2015).									
Statistical and multivariate analyses									
Univariate statistics									
Univariate statistical analyses were conducted to assess differences among sampling sites and site groups and to explore relationships between individual response and predictor variables before multivariate modelling. All statistical analyses were performed using JASP version 0.16.2.0, with Microsoft Excel used for data organization and preliminary visualization.									
Differences among sites or site groups were evaluated using one-way analysis of variance (ANOVA). When significant main effects were detected, Tukey's honest significant difference (HSD) test was applied for post hoc pairwise comparisons. Before analysis, variables were inspected for normality and homogeneity of variance, and transformations were applied where necessary to meet test assumptions.									

Y	nX	R^2X (cum)	R^2Y (cum)	Q^2 (cum)	Regr. intercept Y_{avg}	X variable	Unit	Regr. coefficient (± SE)	VIP (± SE)
Correlation analyses were used to examine covariance between soil carbon stocks and individual predictor variables, including vegetation cover, isotopic signatures, and metal concentrations. These exploratory analyses were used to identify potentially influential predictors and to inform variable selection for subsequent partial least squares regression (PLSR) modelling.									
Partial least squares regression (PLSR)									
Relationships between whole-profile soil C stock (0–20 cm) and biological and geochemical predictors were evaluated using partial least squares regression (PLSR), a multivariate technique suitable for correlated explanatory variables (Wold et al., 2001).									
PLSR was performed in SIMCA version 13.0.3 (Umetrics, Umeå, Sweden). Predictor variables (X) included moss cover, shrub cover, carbon and nitrogen isotopic signatures, and soil trace-metal isotope signatures; whole-profile soil C stock was the sole response variable (Y). PLSR addresses multicollinearity by projecting X onto a limited number of orthogonal latent variables that explain variation in X while maximizing covariance with Y.									
Before modelling, X (moss cover and shrub cover) and Y (total soil carbon stock) variables were examined for normality and transformed (log_{10} for total carbon stock and/or arcsine transformation of moss cover and shrub cover %). All variables were mean-centered and auto-scaled (unit variance scaling) using default SIMCA settings. Model performance and the number of significant PLS components were evaluated using cross-validation (Wold, 1978). In this procedure, subsets of samples were repeatedly excluded from model calibration and predicted by the model built on the remaining samples, yielding cross-validated statistics including Q^2(cum). Q^2(cum) was used to assess model significance and predictive ability and to determine the number of components to retain.									
The importance of individual predictor variables was assessed using Variable Importance for the Projection (VIP) scores and regression coefficient plots. Initial screening considered predictors with VIP values > 0.5 Final PLSR models were constructed by stepwise addition of the most informative predictors to maximize Q^2(cum) while minimizing model complexity. To evaluate the contribution of metal deposition and understory vegetation towards soil carbon formation and storage, final models were compared with and without soil and plant predictors, and changes in model performance were used to assess their relative importance.									

Observed and predicted soil carbon stocks varied among the five site groups along the smelter-impact gradient. It was evident from Fig. 4 that Old Site and Reference observations had consistently positive scores, while New Site and both Intermediate groups had negative scores. Thus, the first latent component clearly separated Old/Reference sites from New/Intermediate sites, although the three negative-score classes overlapped. The x-axis represents observation order rather than a measured variable. The comparison shows that the model broadly reproduces site-level differences and within-site variability in carbon stocks across the 0–20 cm soil profile (Fig. 4).

Methods

Study area

The study was conducted around Gusum (approximately 58°16'N, 16°29'E) in Valdemarsvik Municipality, Östergötland County, southeastern Sweden. The gently undulating landscape lies mostly 40–70 m above sea level, with surrounding high points approaching 100 m; the E22 road passes east of central Gusum (Fig. 1). Mean annual temperature is approximately 5.8°C, and mean annual precipitation is approximately 550 mm.

Vegetation in the study area is dominated by mature mixed coniferous forest, with Norway spruce (*Picea abies* (L.) H.Karst.) as the main tree species, accompanied by Scots pine (*Pinus sylvestris* L.) and birch (*Betula pendula* Roth). Agricultural land use occurs mainly in valley bottoms. In relatively unimpacted stands, the forest floor is typically characterized by continuous bryophyte carpets dominated by feather mosses such as *Hylocomium splendens* (Hedw.) Schimp. and *Pleurozium schreberi* (Willd. ex Brid.) Mitt., together with co-occurring *Dicranum* Hedw. species. In areas affected by long-term Cu and Zn deposition from the Gusum brassworks, previous studies have shown pronounced impacts on forest-floor vegetation, particularly in the bryophyte and lichen layers, as well as expansion of *Deschampsia flexuosa* (L.) Trin. where moss cover is reduced (Folkeson, 1981; Tyler, 1984).

Soils in the region have been classified as Dystric and Eutric Cambisols, as well as Orthic Podzols, according to FAO nomenclature (Almqvist, 2010). Published descriptions of the Gusum area identify veined gneiss as the dominant bedrock type, overlain mainly by podzolized sandy moraine deposits of Quaternary origin (Tyler, 1984). Bedrock geology and Quaternary deposits in the study area were verified using map viewers from the Geological Survey of Sweden (SGU).

Brass production in the Gusum area has occurred almost continuously since 1661. In 1968, the old mill closed, and a new foundry was established 1.6 km to the northwest at Gräsdalen. This long industrial history resulted in sustained atmospheric deposition of copper (Cu), zinc (Zn), and lead (Pb) to surrounding forest ecosystems, while emission controls at the new factory were not introduced until 1982 (Tyler et al., 1984). Although total historical emissions cannot be estimated precisely, approximately 600–700 metric tons of metals were thought to be present in the top 5 cm of soil within 5 km of the two sources. Of this total, about 65% is zinc, 33% is copper, and 2% is lead; nickel, vanadium, and cadmium each account for less than 0.2%. Because the stacks were relatively low, at roughly 20 m, the deposition gradient is steep, and topsoil metal contents returned to background levels about 8 km from the sources (Almqvist, 2010). Soil pH (H_2O) is reported as a range to reflect spatial variability: pH 4.94–5.11 in the organic (mor) layer and pH 4.22–4.97 at a depth of 15–20 cm. These environmental characteristics have been documented in earlier studies of metal deposition, soil contamination, and biological responses in the Gusum forest ecosystems (Folkeson & Andersson-Bringmark, 1988; Langemar, 1994).

Site selection and sampling design

Sampling sites were selected to represent a distance gradient from historical and current brass production sources while minimizing variation in stand structure, slope, aspect, and substrate conditions (Table 1). Site selection was guided by areas investigated in previous studies (Almqvist, 2010; Langemar, 1994) and refined using forest maps to identify mature mixed coniferous stands that had not been harvested since those earlier investigations. To improve comparability among sites, forests were selected on wooded hills with the same bedrock “gneiss-dominated and granite forms” and postglacial deposits, as determined from geological maps, and with high standing tree volume. Only north-facing slopes were included, as south-facing slopes are generally warmer, drier, and more frequently dominated by pine. A reference forest area located approximately 8–10 km from the new factory was included to represent background conditions relative to the emission sources.

At each site, replicate plots were established to capture local heterogeneity in vegetation and soil properties (Supplementary Fig.1). This gradient-based design provided the framework for field surveys and sample collection and allowed us to evaluate how soil carbon (C) storage varied in relation to biological recovery and geochemical contamination under long-term industrial disturbance (Helmisaari, 2001; Rijk & Ekblad, 2020).

The final design comprised forest sites assigned to five groups, grouped based on the distance to the new smelter (within brackets). The groups were *New Site* (<0.5 km), *Old Site* (1-1.2 km), *Intermediate* 1 (1-2 km), *Intermediate* 2 (2-3 km), and *Reference* (7-8 km)—with five to six sampling sites established within each group (Table 1, Figure 1). This structure allowed group-level comparisons along the contamination gradient while retaining within-group replication for vegetation and soil measurements. All sampling points were located at least 200 m from the E22 national highway to minimize potential road-related influences (Table 1).

Field sampling and sample processing

Field survey and soil sampling

Soils, mosses, and spruce needles were sampled during several campaigns between October and November 2022 and in April 2023.

Soil depths were shallow and varied within each site; a metal rod was used to identify areas with soil at least 20 cm deep. Soil samples were collected using a soil corer with an inner diameter of 50 mm. Before coring, the superficial layer of mosses, lichens, and mixed litter was gently removed where present. Soil cores were collected from either three or four directions (based on the topography) around a mature Norway Spruce tree. Each core was divided into 0–5, 5–10, and 10–20 cm intervals, and core sections were pooled in depth intervals, giving a composite sample from 3-4 cores for each depth. Back in the lab, the pooled soil samples were sieved through a 2 mm mesh, and coarse roots and stones were removed by hand.

Collection of moss and spruce needles and assessment of vegetation composition

Targeted moss and spruce-needle sampling and vegetation composition were conducted on 20–21 April 2023, following approaches previously applied in the Gusum area. At each sampling point, the same tree that was used for soil sampling was also visited for needle collection (ca 100 g per tree) and moss sampling. Around the tree, a 5 × 5 m quadrat was established. Within each quadrat, the cover of the dominant moss species *Hylocomium splendens* (Hedw.) Schimp. and *Pleurozium schreberi* (Brid.) Mitt was recorded, while other moss species were grouped as "other." The cover of *Vaccinium myrtillus* L., *Vaccinium vitis-idaea* L., and *Deschampsia flexuosa* (L.) Trin. was also recorded when present.

Moss specimens were collected within 2 m of the centrally located Norway spruce tree in each quadrat. Specimens for laboratory identification were collected separately following standard taxonomic procedures. For chemical analysis, *Hylocomium splendens* (Hedw.) Schimp. was sampled using a fixed-area box (14.4 × 18.4 cm) and stored in airtight polypropylene bags. Stand-structure variables recorded for each quadrat included counts of *Picea abies* (L.) H.Karst. and *Pinus sylvestris* L. trees, basal area, tree height, diameter at breast height, light influx, ground-layer vegetation cover, and visually estimated crown cover.

Stable carbon and nitrogen isotope analyses

Stable carbon ($\delta^{13}C$) and nitrogen ($\delta^{15}N$) isotope compositions were measured for soil and plant materials to characterize organic matter inputs and nitrogen (N) cycling processes and to derive depth-resolved isotope indicators for the statistical analyses.

Carbon (C) and nitrogen (N) concentrations and stable isotope ratios ($\delta^{13}C$ and $\delta^{15}N$) of soil and plant samples were determined using elemental analysis coupled to isotope ratio mass spectrometry (EA-IRMS), following established procedures for ecological and biogeochemical studies (Högberg, 1997; Boström et al., 2007). Freeze-dried soil samples and oven-dried plant materials were finely ground before analysis. Subsamples of approximately 2.5 mg for plant material and 5–10 mg for soil were weighed into tin capsules.

Analyses were conducted using a Vario PYRO cube elemental analyzer (Elementar Analysen system GmbH, Germany) coupled online to an Isoprime precisION isotope ratio mass spectrometer (Elementar UK Ltd.). Carbon and nitrogen isotope ratios are reported in delta notation (‰) relative to Vienna Pee Dee Belemnite (VPDB) for $\delta^{13}C$ and atmospheric N_2 for $\delta^{15}N$, respectively.

Instrument calibration was performed using international reference materials IAEA-CH-6 (sucrose) for carbon and IAEA-N-1 (ammonium sulfate) for nitrogen, consistent with recommended isotope normalization protocols (Craine et al., 2015). Wheat flour was used as a laboratory working standard and analysed repeatedly throughout analytical runs. Analytical precision, expressed as the standard deviation of repeated working-standard measurements, was better than ±0.25‰ for $\delta^{13}C$ and ±0.10‰ for $\delta^{15}N$.

Elemental C and N concentrations were obtained simultaneously during isotope analysis and used for soil C stock calculations, in line with standard approaches for boreal forest soils (Kleja et al., 2008).

Soil C and N stocks for each depth interval were calculated from measured elemental concentrations and oven-dry soil mass per unit area after removal of coarse roots and stones. Whole-profile stocks were obtained by summing the 0–5, 5–10, and 10–20 cm intervals.

Soil and plant metal content analyses

Sample preparation and digestion

Soil samples were freeze-dried, homogenized, and finely ground before digestion. Approximately 0.5 g of soil was digested by microwave-assisted acid digestion using suprapure nitric acid (HNO_3) and hydrochloric acid (HCl), following protocols commonly applied in trace-metal studies of contaminated forest soils (Bindler et al., 1999; Brännvall et al., 2001).

Moss (*Hylocomium splendens* (Hedw.) Schimp.)) and spruce needle samples were gently washed with dilute nitric acid to remove surface contamination, oven-dried, homogenized, and digested using concentrated nitric acid with hydrogen peroxide, following established procedures for vegetation metal analysis near smelters (Folkeson, 1981; Klaminder et al., 2004).

ICP-MS analysis

Metal contents were determined using inductively coupled plasma mass spectrometry (ICP-MS; Agilent 7500 series, Agilent Technologies, Japan). External calibration was performed using multi-element standard solutions spanning the concentration ranges observed in the samples. Rhodium (^{103}Rh) was used as an internal standard to correct for instrumental drift and matrix effects (Supplementary Table 1a).

Quality control included analysis of procedural blanks, replicate digestions, and certified reference materials, consistent with best practice for environmental metal analysis (Bindler et al., 1999; Klaminder, 2004). Instrument performance was monitored through repeated analyses of calibration standards and internal standards throughout analytical sequences.

Total contents of Cu, Zn, and Pb were used as indicators of smelter-derived contamination intensity.

Stable metal isotope analyses

Stable isotope ratios of Cu, Zn and Pb were analysed on selected soil samples to trace contamination sources and mixing between anthropogenic and background metal pools, following established applications of metal isotopes in contaminated forest environments (Brännvall et al., 2001; Wiederhold, 2015).

Zinc isotope ratios are reported as $\delta^{67/66}Zn$ relative to the JMC-Lyon Zn standard, while lead isotope ratios are reported as $^{206/207}Pb$. Instrumental mass bias was corrected using standard–sample bracketing, and analytical reproducibility was assessed through repeated measurements of standards and selected samples (Supplementary Table 1b).

Metal isotope ratios were interpreted as qualitative geochemical tracers of contamination sources and were not used for quantitative mass-balance calculations (Klaminder et al., 2004; Wiederhold, 2015).

Statistical and multivariate analyses

Univariate statistics

Univariate statistical analyses were conducted to assess differences among sampling sites and site groups and to explore relationships between individual response and predictor variables before multivariate modelling. All statistical analyses were performed using JASP version 0.16.2.0, with Microsoft Excel used for data organization and preliminary visualization.

Differences among sites or site groups were evaluated using one-way analysis of variance (ANOVA). When significant main effects were detected, Tukey's honest significant difference (HSD) test was applied for post hoc pairwise comparisons. Before analysis, variables were inspected for normality and homogeneity of variance, and transformations were applied where necessary to meet test assumptions.

Correlation analyses were used to examine covariance between soil carbon stocks and individual predictor variables, including vegetation cover, isotopic signatures, and metal concentrations. These exploratory analyses were used to identify potentially influential predictors and to inform variable selection for subsequent partial least squares regression (PLSR) modelling.

Partial least squares regression (PLSR)

Relationships between whole-profile soil C stock (0–20 cm) and biological and geochemical predictors were evaluated using partial least squares regression (PLSR), a multivariate technique suitable for correlated explanatory variables (Wold et al., 2001).

PLSR was performed in SIMCA version 13.0.3 (Umetrics, Umeå, Sweden). Predictor variables (X) included moss cover, shrub cover, carbon and nitrogen isotopic signatures, and soil trace-metal isotope signatures; whole-profile soil C stock was the sole response variable (Y). PLSR addresses multicollinearity by projecting X onto a limited number of orthogonal latent variables that explain variation in X while maximizing covariance with Y.

Before modelling, X (moss cover and shrub cover) and Y (total soil carbon stock) variables were examined for normality and transformed (log_{10} for total carbon stock and/or arcsine transformation of moss cover and shrub cover %). All variables were mean-centered and auto-scaled (unit variance scaling) using default SIMCA settings. Model performance and the number of significant PLS components were evaluated using cross-validation (Wold, 1978). In this procedure, subsets of samples were repeatedly excluded from model calibration and predicted by the model built on the remaining samples, yielding cross-validated statistics including Q^2(cum). Q^2(cum) was used to assess model significance and predictive ability and to determine the number of components to retain.

The importance of individual predictor variables was assessed using Variable Importance for the Projection (VIP) scores and regression coefficient plots. Initial screening considered predictors with VIP values > 0.5 Final PLSR models were constructed by stepwise addition of the most informative predictors to maximize Q^2(cum) while minimizing model complexity. To evaluate the contribution of metal deposition and understory vegetation towards soil carbon formation and storage, final models were compared with and without soil and plant predictors, and changes in model performance were used to assess their relative importance.

Discussion

Across the Gusum smelter landscape, soil carbon (C) stocks varied more than fourfold and did not follow a simple gradient with distance from the active smelter or absolute metal contents. High soil C stocks occurred at the reference and old smelter sites, whereas the new smelter and intermediate sites had comparably low stocks despite their contrasting contamination histories. These spatial patterns indicate that residual metal loads alone do not explain contemporary variation in soil C storage.

The multivariate analyses reinforce this interpretation. The vertical structure of soil $\delta^{15}N$ had the highest variable-importance score in the final model, while combining one of the predictors with moss and shrub cover provided additional predictive information. Two metal isotope variables were also retained, but each had a lower variable-importance score than the $\delta^{15}N$ slope. Together, these results suggest that biological structure and depth-resolved isotope patterns were more informative for explaining soil C stocks than metal contents alone. This interpretation is consistent with earlier work in smelter-affected boreal systems showing that metal pollution can influence soil C storage indirectly through changes in vegetation structure and nutrient cycling (Hutchinson & Whitby, 1977; Helmisaari, 2001; Rijk & Ekblad, 2020).

The observation that intermediate sites exhibited low soil C stocks despite lower surface contamination than sites closer to the new smelter further supports the notion that ecosystem recovery trajectories are controlled by the re-establishment of biological structure rather than by contamination gradients per se. Together, these results emphasize that recovery of soil C storage reflects ecosystem-level reorganization rather than simple release from chemical stress.

Among all predictors examined, the vertical gradient of soil $\delta^{15}N$ emerged as one of the strongest predictors of soil C storage. Sites with steeper $\delta^{15}N$ gradients tended to exhibit higher soil C stocks, whereas intermediate sites with shallow gradients consistently exhibited low C storage.

This depth-resolved $\delta^{15}N$ signal likely reflects long-term integration of organic matter inputs and nitrogen (N) cycling processes rather than short-term changes in surface conditions. Depth enrichment of $\delta^{15}N$ is a widely observed feature of forest soils and arises from a combination of fractionating N transformations and changing contributions of plant-derived and microbial-derived organic matter with depth (Högberg, 1997; Hobbie & Ouimette, 2009; Kramer et al., 2017). Importantly, the strong association between $\delta^{15}N$ gradients and soil C stocks observed here does not require invoking intensified N processing rates per se. Instead, it is consistent with changes in the relative contribution of isotopically distinct litter sources —particularly low-$\delta^{15}N$ moss litter at the surface and higher-$\delta^{15}N$ root and mycorrhizal inputs at depth—as vegetation structure recovers.

Integrating vegetation composition, litter inputs, and long-term N transformations, depth-resolved soil $\delta^{15}N$ provides a robust, process-relevant indicator of ecosystem recovery that cannot be inferred from bulk or surface isotope measurements alone. This supports previous syntheses identifying soil $\delta^{15}N$ profiles as stronger indicators of ecosystem N cycling state than plant $\delta^{15}N$ in forest systems (Templer et al., 2007; Liao et al., 2021).

Soil concentrations of Cu, Zn, and Pb, as well as stable Zn and Pb isotope ratios, clearly documented the legacy and spatial structure of smelter-derived contamination across the Gusum landscape. Metal isotope signatures effectively traced contamination sources and mixing between anthropogenic and background pools, confirming their utility as tracers of pollution history.

However, neither absolute metal contents nor metal isotope ratios displayed a strong direct association with soil C stocks once biological and isotopic indicators of ecosystem functioning were considered. In multivariate models, two metal isotope variables were retained, indicating a secondary but detectable contribution, but they did not displace the $\delta^{15}N$ slope or vegetation metrics as the dominant predictors. This indicates that while contamination history remains detectable, its influence on contemporary soil C storage is largely indirect and context dependent.

These findings are consistent with studies showing that heavy metals primarily affect soil C dynamics through suppression of vegetation and microbial functioning rather than through direct stabilization or destabilization of soil organic matter (Helmisaari, 2001; Xu et al., 2021; Rabow et al., 2022). Metal isotopes thus remain valuable tools for reconstructing disturbance histories but provide limited mechanistic insight into ecosystem C storage unless interpreted alongside biological recovery indicators.

Moss cover exhibited a strong spatial correspondence with soil C stocks across the Gusum gradient, with near-continuous bryophyte carpets at reference and old smelter sites and sparse or heterogeneous moss cover at sites with low C storage.

This pattern is consistent with a growing body of literature highlighting the disproportionate role of bryophytes in regulating boreal forest-floor microclimate, decomposition, and organic matter stabilization (Lindo & Gonzalez, 2010; Turetsky et al., 2012).

Feather mosses such as *Hylocomium splendens* and *Pleurozium schreberi* contribute substantial litter inputs that decompose slowly, insulate soil against temperature extremes, maintain high moisture conditions, and modify microbial activity (Tamm, et al., 1953). Kasimir et al. (2021) likewise showed that mosses enhance soil carbon sequestration in boreal peatlands by producing slowly decomposing litter, maintaining high soil moisture, and reducing drought-related carbon losses. Experimental removal of moss layers has repeatedly been shown to accelerate litter decomposition and alter soil C and N dynamics (Lindo & Gonzalez, 2010; Grau-Andrés et al., 2022). The close association between moss recovery and soil C storage observed in this study therefore aligns with established bryosphere-mediated controls on boreal biogeochemistry (Eldridge et al., 2023).

At the same time, shrub cover exhibited a similar predictive contribution in the multivariate models, underscoring that soil C recovery reflects broader re-establishment of forest-floor and understory structure rather than moss recovery in isolation. Together, these results suggest that mosses act as a key—but not exclusive—component of a recovering vegetation matrix that promotes long-term soil C accumulation.

Several limitations should be considered when interpreting these patterns. The study is based on an observational spatial gradient, so the reported associations do not by themselves establish causal effects of vegetation recovery, isotope structure, or metal legacies on soil C storage. The number of sites and within-site samples also constrains the complexity and external validation of the PLSR model. In addition, unmeasured differences in stand history, microtopography, soil development, or past disturbance may contribute to among-site variation. The results should therefore be viewed as evidence for candidate indicators and mechanisms that require testing across independent smelter-affected landscapes and, where possible, through longitudinal or experimental studies.

This study has broader implications for assessing ecosystem recovery under chronic anthropogenic disturbance. Indicators that integrate biological structure and long-term nutrient cycling —rather than static measures of contamination—may provide more reliable measures and assessments of ecosystem functioning and resilience than static contamination metrics. In particular, depth-resolved stable isotope profiles offer a powerful yet underutilized tool for linking vegetation recovery to soil C dynamics in boreal and temperate forests. And multivariate analyses help identify complementary features that provide additional key information about how these complex structural roles of biological and geochemical indicators play in restoration and ecosystem balance.

Conclusions

Along the Gusum contamination gradient, whole-profile soil C stocks varied more than fourfold but did not follow a simple distance-to-source or contamination-load pattern. Instead, variation in soil C storage was most strongly associated with forest-floor vegetation structure and depth-resolved indicators of long-term biogeochemical functioning.

Among the predictors examined, the vertical gradient of soil $\delta^{15}N$ emerged as one of the most informative integrative indicators of soil C storage, capturing the cumulative imprint of vegetation inputs, organic matter processing, and nitrogen cycling with depth. Its association with soil C stocks highlights the value of depth-resolved isotope profiles for assessing long-term ecosystem functions in disturbed forest systems. Unlike surface measurements alone, these profiles reflect coupling between C and N dynamics through the soil profile and provide insight into ecosystem functioning.

Higher soil C storage was also associated with recovery of forest-floor vegetation, particularly moss-dominated ground layers. Moss and shrub cover contributed complementary explanatory information, indicating broad biological reassembly rather than an isolated effect of one vegetation component. Metal contents and isotope signatures traced contamination history but added less direct explanatory power once biological and depth-resolved isotopic indicators were considered.

More broadly, the study shows that biologically grounded indicators—particularly vegetation structure and depth-resolved stable isotope patterns—provide robust, process-relevant measures of ecosystem recovery under chronic anthropogenic disturbance. Such indicators may be essential for assessing the resilience and long-term carbon sink potential of forest ecosystems in a changing world.

Declarations

Competing interests

The authors declare no competing interests.

Funding

The position of L.G. was funded by the Knowledge Foundation of Sweden [grant number 20200270]

The position of I.R. was funded to A.E. from Structor Miljoteknik AB, the Faculty Board of Business, Science and Engineering of Orebro University, and the Knowledge Foundation of Sweden [grant number 20200270].

Author Contribution

LG: Conceptualization, methodology, investigation, formal analysis, data curation, visualization, writing—original draft. IR: Sampling, writing—review and editing. DBK: Supervision, conceptualization, methodology, writing—review and editing. MZ: Sampling, formal analysis, writing—review and editing. VS: Formal analysis, writing—review and editing. AE: Conceptualization, methodology, investigation, formal analysis, data curation, visualization, writing—original draft, supervision, project administration, and funding acquisition. All authors reviewed the manuscript.

Acknowledgement

Authors acknowledge support received from Sussane Karlsson and Ebba Wadstein, Structor Miljö Öst AB, Linköping, for preliminary field information and site visits. Annett Köllman for administrative support and the remediation report, and Hanna Almqvist for sharing the historical background. Hanna Landen and Elvira for laboratory assistance. Tao Zhao for economic guidance. Örebro University, Örebro for institutional or technical support.

Data Availability

No custom code was developed for this study. Data organization and preliminary visualization were performed in Microsoft Excel; univariate analyses were conducted in JASP version 0.16.2.0; and partial least squares regression analyses were performed in SIMCA (Umetrics) version 13.0.3 using the procedures described in the Methods. Analysis-ready input data and the model settings needed to reproduce the reported analyses are available from the corresponding author upon reasonable request.

References

1. Almqvist, H. (2010). *The legacy of the mill: A metal-polluted forest soil in Gusum*. Master's thesis, Swedish University of Agricultural Sciences, Uppsala, Sweden.

2. Angst, S. et al. Un(der)explored links between plant diversity and particulate and mineral-associated organic matter in soil. *Nature Communications* (2025). https://doi.org/10.1038/s41467-025-60712-6.
3. Bindler, R., Bränvall, M.-L., Renberg, I., Emteryd, O. & Grip, H. Natural lead concentrations in pristine boreal forest soils and past pollution trends: a reference for critical load models. *Environmental Science & Technology* 33, 3362–3367 (1999).
4. Boström, B., Comstedt, D. & Ekblad, A. Isotope fractionation and 13C enrichment in soil profiles during the decomposition of soil organic matter. *Oecologia* 153, 89–98 (2007). https://doi.org/10.1007/s00442-007-0700-8.
5. Brännvall, M.-L., Bindler, R., Emteryd, O. & Renberg, I. Stable isotope signatures of lead in atmospheric deposition and soils in northern Europe. *Environmental Science & Technology* 35, 4679–4686 (2001).
6. Craine, J. M. et al. Ecological interpretations of nitrogen isotope ratios of terrestrial plants and soils. *Plant and Soil* 396, 1–26 (2015).
7. Eldridge, D. J. et al. The global contribution of soil mosses to ecosystem services. *Nature Geoscience* 16, 430–438 (2023). https://doi.org/10.1038/s41561-023-01170-x.
8. Folkeson, L. Impact of airborne copper and zinc pollution on lichen and bryophyte vegetation near a brass foundry. *Silva Fennica* 15, 446–449 (1981).
9. Folkeson, L. Deterioration of the moss and lichen vegetation in a forest polluted by heavy metals. *Ambio* 13, 37–39 (1984).
10. Folkeson, L. & Andersson-Bringmark, E. Impoverishment of vegetation in a coniferous forest polluted by copper and zinc. *Canadian Journal of Botany* 66, 417–428 (1988).
11. Grau-Andrés, R., Wardle, D. A. & Kardol, P. Bryosphere loss impairs litter decomposition consistently across moss species, litter types, and micro-arthropod abundance. *Ecosystems* 25, 1542–1554 (2022). https://doi.org/10.1007/s10021-021-00731-8.
12. Helmisaari, H.-S. Areas polluted by heavy metals. In *Forest Condition in a Changing Environment* (ed. Paoletti, E.) 248–251 (Springer, 2001).
13. Hobbie, E. A. & Ouimette, A. P. Controls of nitrogen isotope patterns in soil profiles. *Ecosystems* 12, 1164–1177 (2009).
14. Högberg, P. 15N natural abundance in soil–plant systems. *New Phytologist* 137, 179–203 (1997). https://doi.org/10.1046/j.1469-8137.1997.00808.x.
15. Hutchinson, T. C. & Whitby, L. M. The effects of acid rainfall and heavy metal particulates on a boreal forest ecosystem near the Sudbury smelting region of Canada. *Water, Air, and Soil Pollution* 7, 421–438 (1977). https://doi.org/10.1007/BF00285542.
16. Kasimir, A., He, H., Jansson, P.-E., Lohila, A. & Minkkinen, K. Mosses are important for soil carbon sequestration in forested peatlands. *Frontiers in Environmental Science* 9, 680430 (2021). https://doi.org/10.3389/fenvs.2021.680430.
17. Klaminder, J., Bindler, R., Emteryd, O. & Renberg, I. Isotopic composition of atmospheric lead pollution in Sweden. *Environmental Science & Technology* 38, 1017–1023 (2004).
18. Kleja, D. B. et al. Pools and fluxes of carbon in three Norway spruce ecosystems along a climatic gradient in Sweden. *Biogeochemistry* 89, 7–25 (2008). https://doi.org/10.1007/s10533-007-9136-9.
19. Kögel-Knabner, I. & Amelung, W. Dynamics, chemistry, and preservation of organic matter in soils. In *Organic Geochemistry* 157–215 (Elsevier, 2013). https://doi.org/10.1016/B978-0-08-095975-7.01012-3.
20. Kramer, M. G., Lajtha, K. & Aufdenkampe, A. K. Depth trends of soil organic matter C:N and δ15N reflect long-term plant inputs and processing. *Soil Biology & Biochemistry* 105, 112–123 (2017).
21. Langemar, O. (1994). *Environmental monitoring of metal deposition and soil contamination in the Gusum area*. Report by Lund University and Kjessler & Mannerstråle AB, Sweden.
22. Liao, K., Lai, X. & Zhu, Q. Soil δ15N is a better indicator of ecosystem nitrogen cycling than plant δ15N: a global meta-analysis. *Biogeochemistry* 153, 199–213 (2021).

23. Lindo, Z. & Gonzalez, A. The bryosphere: an integral and influential component of the Earth's biosphere. *Ecosystems* 13, 612–627 (2010). https://doi.org/10.1007/s10021-010-9336-3.
24. Rabow, S., Soares, M. & Rousk, J. Heavy metal pollution suppresses decomposer functioning in forest soils. *Microbial Ecology* 83, 858–870 (2022).
25. Rijk, I. J. C. & Ekblad, A. Carbon and nitrogen cycling in a lead-polluted grassland evaluated using stable isotopes and microbial, plant and soil parameters. *Plant and Soil* 449, 249–266 (2020). https://doi.org/10.1007/s11104-020-04467-7.
26. Rijk, I. J. C., Zeiner, M., Kleja, D. B., Goswami, L. & Ekblad, A. Total copper explains variation in soil organic carbon accumulation but not in situ soil respiration: an ecosystem evaluation of a century-old wood impregnation site. *Environmental Toxicology and Chemistry*, vgag155 (2026). https://doi.org/10.1093/etojnl/vgag155.
27. Rocci, K. S. et al. Aligning theoretical and empirical representations of soil carbon-to-nitrogen stoichiometry with process-based terrestrial biogeochemistry models. *Soil Biology and Biochemistry* (2024). https://doi.org/10.1016/j.soilbio.2023.109272.
28. Tamm, C. O. *Growth, Yield and Nutrition in Carpets of a Forest Moss (Hylocomium splendens)*. Meddelanden från Statens Skogsforskningsinstitut 43, 1–140 (1953).
29. Templer, P. H., Arthur, M. A., Lovett, G. M. & Weathers, K. C. Plant and soil δ15N as indicators of nitrogen cycling rates in temperate forests. *Biogeochemistry* 84, 297–313 (2007). https://doi.org/10.1007/s10533-007-9138-7.
30. Turetsky, M. R. et al. The resilience and functional role of moss in boreal and arctic ecosystems. *New Phytologist* 196, 49–67 (2012).
31. Tyler, G. Impact of heavy metal pollution on forests: a case study of Gusum, Sweden. *Ambio* 13, 18–24 (1984).
32. Wiederhold, J. G. Metal stable isotope signatures as tracers in environmental geochemistry. *Reviews in Mineralogy and Geochemistry* 82, 1–30 (2015).
33. Wold, S. Cross-validatory estimation of the number of components in factor and principal components models. *Technometrics* 20, 397–405 (1978). https://doi.org/10.1080/00401706.1978.10489693.
34. Wold, S., Sjöström, M. & Eriksson, L. PLS-regression: a basic tool of chemometrics. *Chemometrics and Intelligent Laboratory Systems* 58, 109–130 (2001).
35. Xu, M., Rousk, J., Li, H. & Zhang, Y. Heavy metal pollution increases soil microbial carbon limitation. *Soil Biology & Biochemistry* 156, 108227 (2021).

Figures

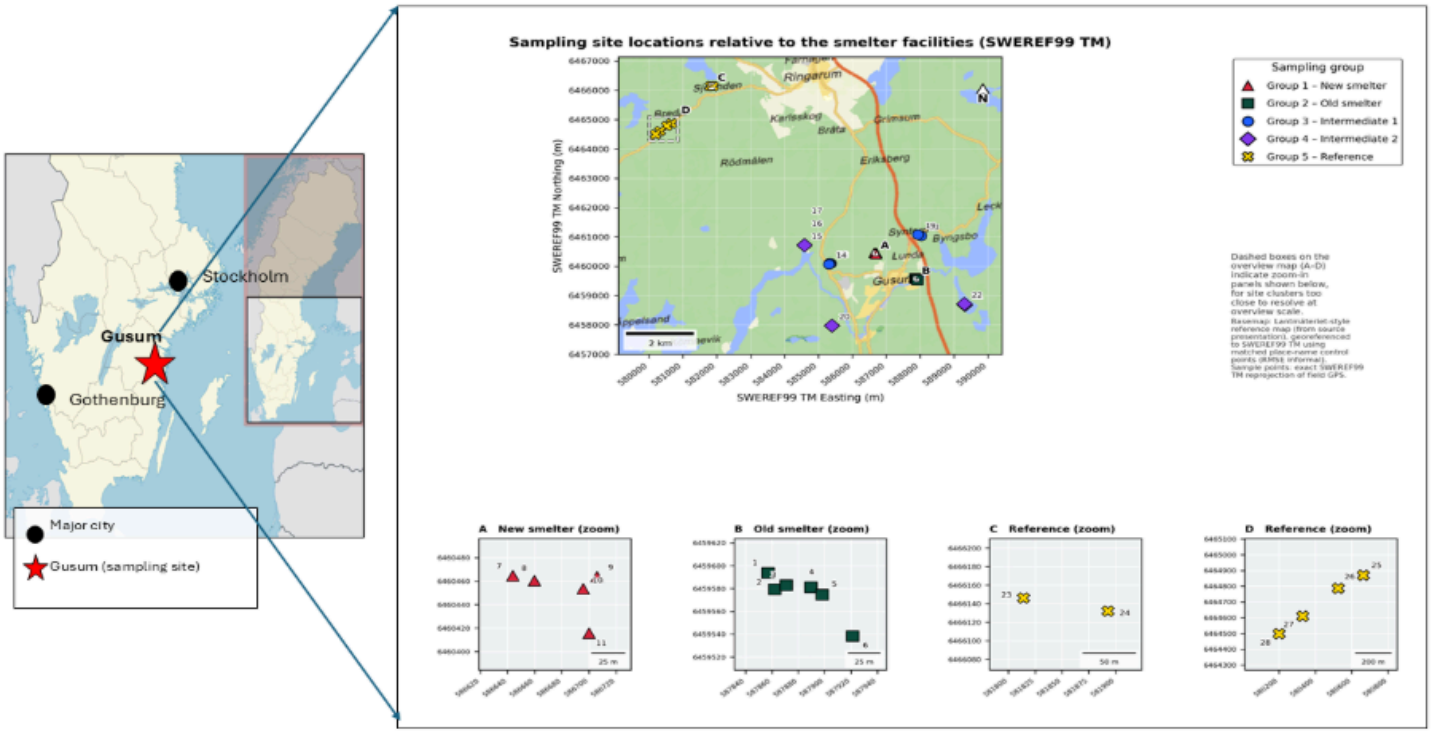


Figure 1

Study design and sampling locations around the Gusum brassworks, southeastern Sweden. The map shows the old and new smelters, the five site groups used in the analysis (New Site, Old Site, Intermediate 1, Intermediate 2, and Reference), and replicate sampling points. Site groups represent the spatial contamination gradient; coordinates, distances, and bearings relative to the new smelter are provided in Table 1.

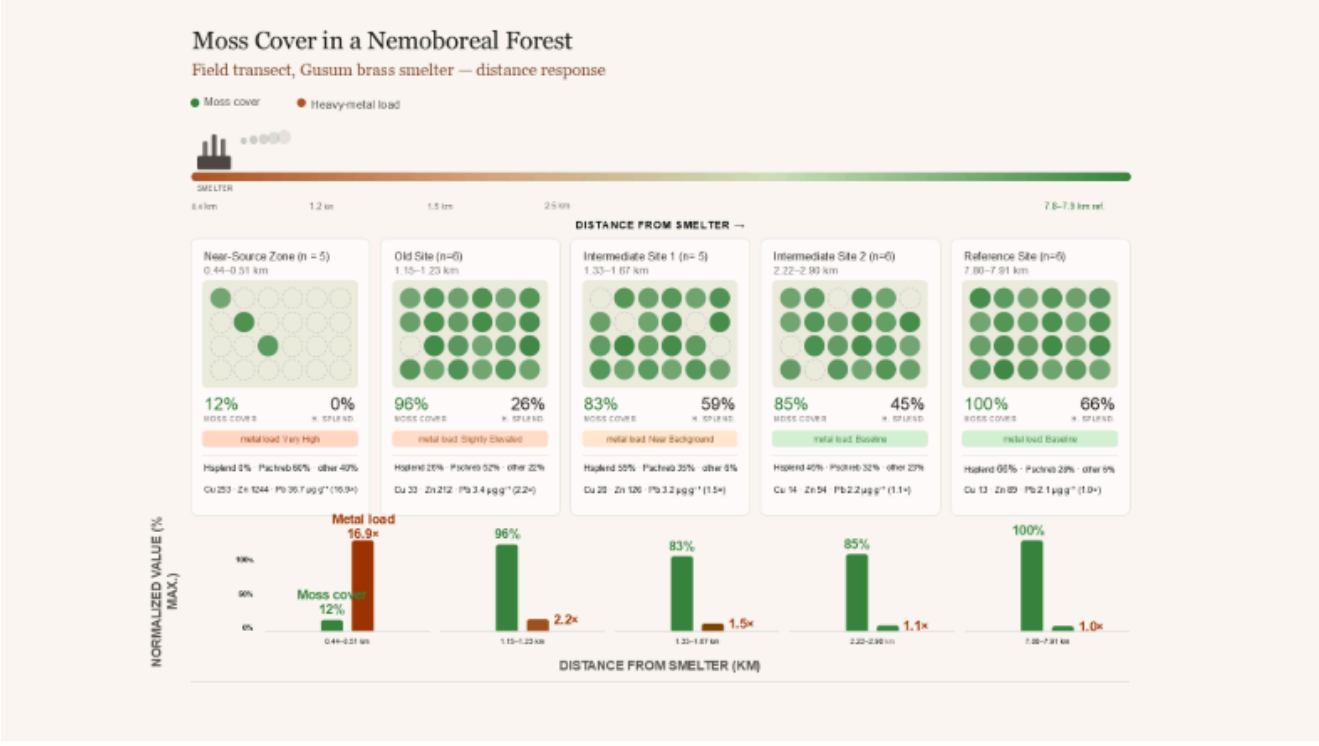


Figure 2

Representative ground-layer vegetation at sites along the smelter-impact gradient. Photographs illustrate differences in forest-floor structure among site groups, from sparse or heterogeneous bryophyte cover near the new smelter and at intermediate sites to continuous feather-moss carpets at the Old and Reference Sites. Dominant mosses at high-cover sites included Hylocomium splendens and Pleurozium schreberi. Site labels and scale references are shown within each panel.

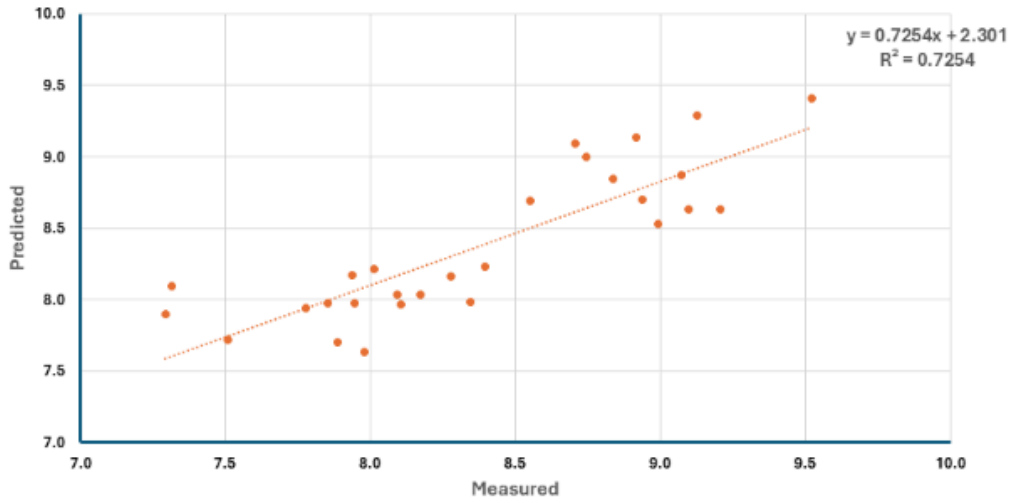


Figure 3

Observed and cross-validated predicted whole-profile soil carbon stocks from the final partial least squares regression model. The response variable was ln-transformed soil C stock integrated over 0–20 cm. The final model included soil $\delta^{15}N$ slope, $\delta^{67}/^{66}Zn$,δ $^{206}Pb/^{207}Pb$, moss cover, and shrub cover. Symbols represent individual samples. Model statistics were R^2Y = 0.725 and Q^2 = 0.685.

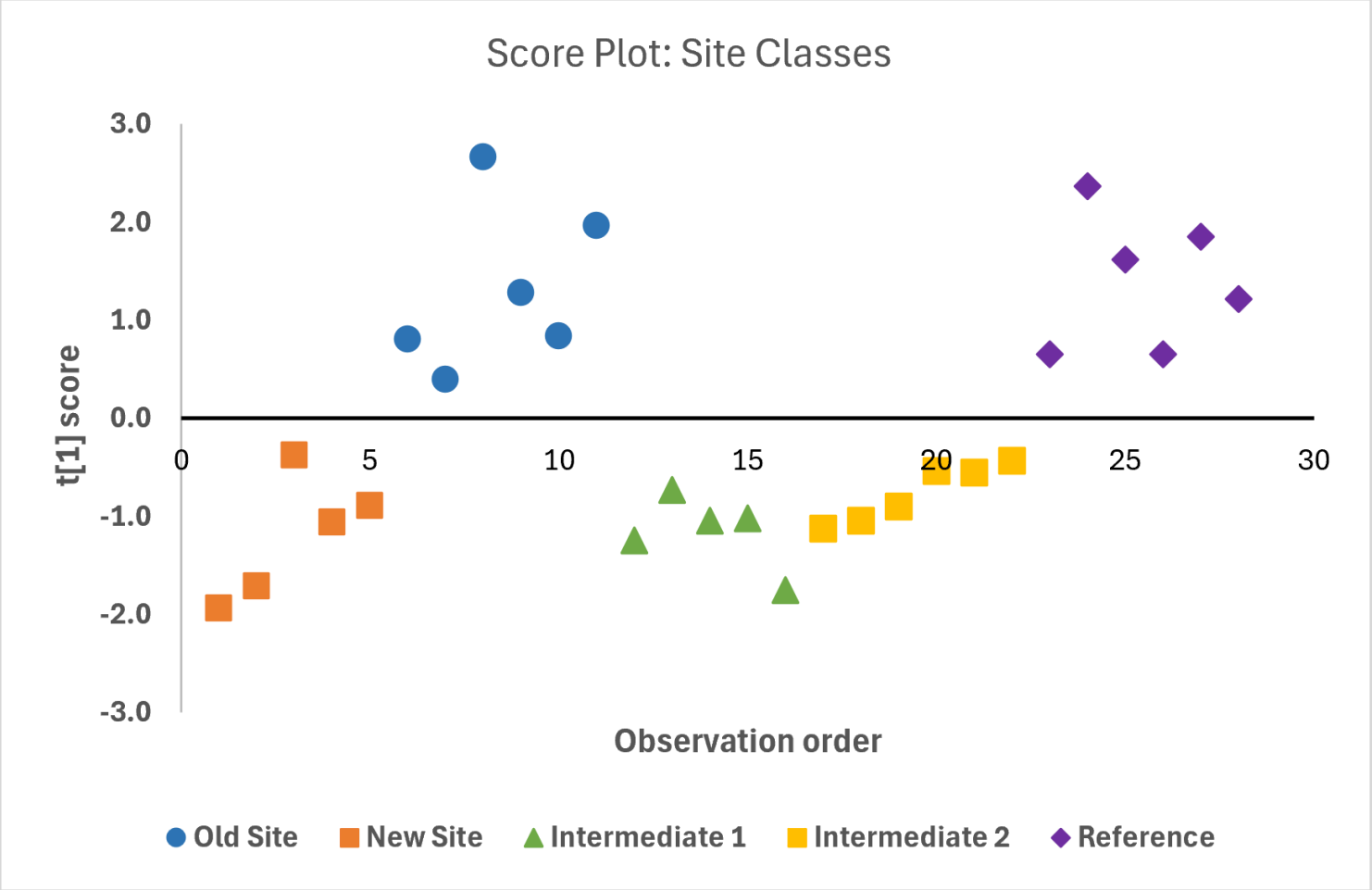


Figure 4

Score plot of the model with the highest Q2 (only one PLS component was significant). The number on the Y-axis (the t1-score) is summarizing the X-variables among the sites (objects), and objects that are closer to each other are more similar. Note that the X-axis is just an observation with no value. Individual points represent sites; colors identify site groups.

Supplementary Files

This is a list of supplementary files associated with this preprint. Click to download.

- 020926SupplementarytablesNPJSE.pdf
- 03092026SupplementaryFiguresnewNPJSE.pdf